

Quasi-Static Deformation of a Granular System with a Regular Arrangement of Particles

So Kitsunezaki

Abstract In order to study the growth of heterogeneity in granular systems, we investigate the quasi-static deformation of monodisperse particle systems with regular initial arrangements. We construct a linearized model by limiting our consideration to infinitesimal deformations. Assuming Coulomb friction, we introduce new variables to express the slippage distances of particles in contact. The results of our numerical simulations show that heterogeneities appear through a fingering-like instability and develop into several microscopic shear zones. The equations in our model can be reduced to simpler equations in the limit of small tangential interactions using a perturbative analysis. In the long wavelength limit, the equations are analogous to models of Laplacian growth, such as the dielectric breakdown problem. We investigate the instability of critical stress states and the competitive growth of microscopic shear zones.

Key words. quasi-static deformation, shear bands, faults, sand-box experiments, fingering instability

1

Introduction

When a compression or shear strain is applied to a static granular system, several shear bands develop and, eventually, fracture the system. Such a macroscopic response to externally applied forces is similar to that exhibited by elastic and plastic materials. For this reason, macroscopic shear bands appearing in granular materials have been studied with the use of elastic theories combined with an empirical breaking condition, such as the Mohr-Coulomb criterion, and elasto-plastic theories [1–3]. However, microscopically, granular materials are qualitatively different from usual solids. In particular, constituent particles in granular systems are insensitive to thermal fluctuations, and any deformation of a static granular system is inevitably accompanied by energy dissipation due to frictional interactions among particles. The stress state of a granular system depends significantly on the history of its formation [4–9]. In order to understand the creation mechanism of shear bands in granular systems, we need to study the dynamics of the constituent particles [10–17].

Here, we theoretically investigate shear bands in cohesionless granular systems subject to quasi-static deformation. We consider so-called “sand-box” experiments. In a general sand box experiment, a system of dry sand held in a container is deformed slowly by moving one of the lateral walls of the container. Systems of this type have been studied as simple models of geophysical faults [18–20], and the results of such experiments reveal that a series of parallel shear bands are created sequentially in many kinds of granular systems, ranging from sand to nearly monodisperse glass beads.

In a previous work [21], with an experimental study, we carried out 2-dimensional numerical simulations of monodisperse granular systems with regular initial arrangements using the discrete elements method (DEM) [22]. We investigated the time development of the stress field before the creation of shear bands and found that when a shear deformation is applied to these systems, a fingering-like instability is created in the stress field, and many microscopic shear bands appear. These bands first appear near the top surface of the system and then begin to grow downward. In this process, the bands compete, and through this competition, only a few of the initial bands are selected and grow to ‘macroscopic’ size. The growth of these shear bands eventually breaks the regular arrangement of particles, as they come to form a series of faults running through the system. As a result of the competition of microscopic shear bands, the spacing between neighboring faults increases with their length. We noted that the series of faults in such idealized system are similar to those observed in experiments although they are different in the thickness of a fault.

In this paper, we theoretically investigate the initial response of such regular granular systems to deformation. Although a fault in regular granular systems is a kind of dislocation, its creation process can not be understood on the ground of the statistical physics in contrast with that of an atomic-scale dislocation. The static properties and dynamical behavior of granular systems with regular arrangements has been investigated recently in several studies [23–27]. In the present work, we are here interested in the dynamics of quasi-static deformation of such systems.

In Sec. 2, we propose a linearized model that is constructed by considering the infinitesimal deformation of regular arrangements of particles. We describe the Coulomb friction among particles by using new variables to express the slippage distances of particles in contact. In Sec. 3, we report that a fingering-like instability of the stress field is also observed in numerical simulations of this model. In

So Kitsunezaki

Department of Physics, Graduate School of Human Culture,
Nara Women’s University, Nara 630-8506.
e-mail: kitsune@ki-rin.phys.nara-wu.ac.jp

Sec. 4 we reduce our model to a system of simpler equations in the limit of small tangential interactions using a perturbative analysis. We elucidate the qualitative nature of the mechanism controlling the competitive growth of microscopic shear zones and carry out a the stability analysis of critical stress states employing the form taken by the reduced equations in the long-wavelength limit.

2

Linearized model for infinitesimal deformation

In this section we introduce a model describing the infinitesimal deformation of 2-dimensional monodisperse granular systems with regular arrangements. We consider disks of radius a and mass m as particles and stack them in a V-shaped container, as depicted in Fig. 1. The V-shaped container is oriented so that the axis x bisecting it is tilted by ϕ_g degrees with respect to the direction of gravity. We apply a uniform shear deformation to the system by opening the walls of the V-shaped container quasi-statically.

We investigated this system numerically using DEM simulations in a previous work [21]. In that case, we used an equilateral triangular arrangement of particles as the initial arrangement. We found that as the walls are opened, the state of smooth deformation becomes unstable, so that many microscopic shear zones appear in the stress field. At this stage, the displacement of every particle is smaller than the particle size. Therefore a microscopic shear zone is neither a fault nor a shear band in the usual sense. It may be interpreted as a kind of “microband” called by Kuhn [15]. As a result of the growth of these microscopic shear zones, macroscopic faults are created as faults in the arrangement of particles. Both the microscopic shear zones and the resultant faults appear in a series of V-shaped forms if $\phi_g = 0$, while as ϕ_g increases, the faults eventually take the form of a series of lines along one direction.

When the microscopic shear zones appear, the number of contact points is 4 for most particles. The horizontal contacts existing initially among particles are so weak that, as soon as the walls begin to open, they are lost due to the Reynolds dilatancy [28]. We found that the above-stated results of the DEM simulations are unchanged if instead of the equilateral triangular arrangement used in

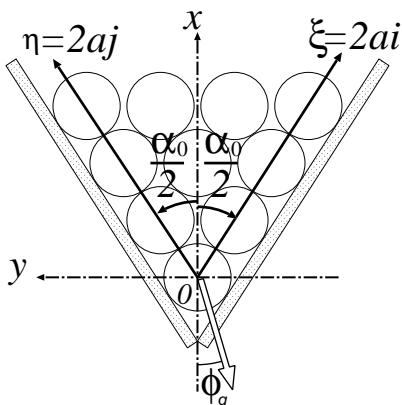


Fig. 1. The initial arrangement of particles.

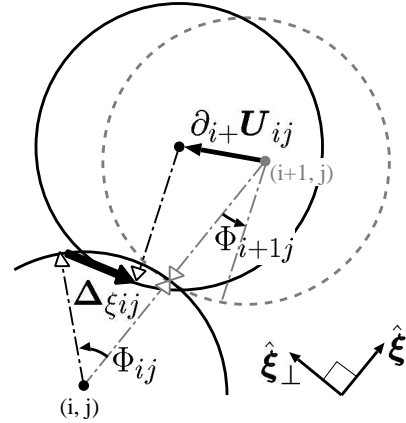


Fig. 2. The relative displacement of particles in contact.

The dotted circle represents the particle $(i+1, j)$ in the initial state. Its center moves by $2a\delta_{i+}U_{ij} \equiv U_{i+1j} - U_{ij}$ with respect to the particle (i, j) , and both the particles rotate by Φ_{i+1j} and Φ_{ij} respectively. The symbol \bowtie indicates the initial contact point. The corresponding points on both the particles move to the positions indicated by \triangleright and \triangleleft respectively.

previous studies we employ a rhombic arrangement composed of nearly equilateral triangles. We believe that such a rhombic arrangement is more fundamental in these deformation processes, as it is more generic than the closest-packing structure studied previously. In this study, we consider systems with rhombic initial arrangements and assume that the set of particles representing the nearest neighbors of any given particle remains unchanged during the small deformation process.

In cohesionless granular systems whose particles are subject to elastic forces in contact, the free energy of the system is equal to the sum of the elastic energies and the gravitational potential energies of all particles. We conjecture that the system remains in an equilibrium state, minimizing this free energy, when the boundary conditions are changed quasi-statically. In order to construct the free energy, we linearize the elastic forces by assuming that the relative displacements of particles in contact are sufficiently smaller than the particle size. We assume Coulomb friction to exist at every contact among the particles. Slip occurs at a contact point when the magnitude of the tangential component of the elastic force increases beyond the maximal static frictional force with coefficient μ . We introduce new variables into the free energy to express slip displacements. As the boundary conditions of the system change quasi-statically, the slip displacements are assumed to change slightly at every time that the Coulomb condition is broken at any contact in such a manner that these conditions are restored.

We introduce the reference coordinates (ξ, η) along the walls in the initial state, as depicted in Fig. 1, where α_0 indicates the angle between the two axes. $\hat{\xi}$ and $\hat{\eta}$ represents the unit vectors in the ξ and η directions. Particles are positioned at $\mathbf{x}_{ij} \equiv 2a(i\hat{\xi} + j\hat{\eta})$ when every particle is in contact without deformation, where $2a$ is the diameter of a particle, and i and j are integers. We refer to each particle on the rhombic lattice by the corresponding site

(i, j) . Each particle remains in contact with its 4 nearest neighbors while it translates and rotates. The quantities \mathbf{U}_{ij} and Φ_{ij} represent the displacement and the rotation angle, respectively, of the particle (i, j) . We express the components of \mathbf{U}_{ij} as $U_{ij} \equiv \hat{\xi} \cdot \mathbf{U}_{ij}$ and $V_{ij} \equiv \hat{\eta} \cdot \mathbf{U}_{ij}$. Defining the perpendicular unit vectors $\hat{\eta}_\perp$ and $\hat{\xi}_\perp$ by $\hat{\xi} \cdot \hat{\xi}_\perp = \hat{\eta} \cdot \hat{\eta}_\perp = 0$ and $\hat{\xi} \cdot \hat{\eta}_\perp = \hat{\eta} \cdot \hat{\xi}_\perp = \sin \alpha_0$, the displacement can be written

$$\mathbf{U}_{ij} = \frac{1}{\sin \alpha_0} (U_{ij} \hat{\eta}_\perp + V_{ij} \hat{\xi}_\perp). \quad (1)$$

We construct the free energy of the system as a function of $(U_{ij}, V_{ij}, \Phi_{ij})$, assuming that $U_{ij}, V_{ij} \ll a$ and $\Phi_{ij} \ll 1$. As in the DEM, we represent the elastic forces on each contact point by two linear springs acting in the normal and tangential directions with spring constants k_n and k_t , respectively. In order to determine the elastic deformations of the springs, we consider the contact of two disks to result not in mutual deformation but, rather, overlap. Treating the particle-particle interaction in this manner simplifies the model, while we believe that employing a more realistic deformation would not alter the results significantly. We consider the two contacts of the particle (i, j) at which it contacts the particles $(i+1, j)$ and $(i, j+1)$. As shown in Fig. 2, the relative displacements for these contacts are given by

$$\begin{cases} \Delta_{\xi ij} \equiv 2a\partial_{i+}U_{ij} - a(\Phi_{ij} + \Phi_{i+1j})\hat{\xi}_\perp \\ \Delta_{\eta ij} \equiv 2a\partial_{j+}U_{ij} + a(\Phi_{ij} + \Phi_{ij+1})\hat{\eta}_\perp \end{cases}, \quad (2)$$

to linear order. Here, we have defined $\partial_{i\pm}A_{ij} \equiv \pm(A_{i\pm 1j} - A_{ij})/2a$ and $\partial_{j\pm}A_{ij} \equiv \pm(A_{ij\pm 1} - A_{ij})/2a$. We interpret the normal components $\Delta_{\xi ij} \cdot \hat{\xi}$ and $\Delta_{\eta ij} \cdot \hat{\eta}$ as the displacements of the normal springs. In contrast, the tangential component at each contact is assumed to be the sum of the elongation of the tangential spring and the slip displacement. We introduce the new variables to represent $\Psi_{\xi ij}$ and $\Psi_{\eta ij}$ to express the slip displacements divided by the particle diameter $2a$, and interpret $\Delta_{\xi ij} \cdot \hat{\xi}_\perp - 2a\Psi_{\xi ij}$ and $\Delta_{\eta ij} \cdot \hat{\eta}_\perp + 2a\Psi_{\eta ij}$ as the displacements of the tangential springs. Therefore, the elastic forces acting on the respective contacts of the particle (i, j) are expressed as

$$\mathbf{f}_{\xi ij} \equiv 2a(k_n N_{\xi ij} \hat{\xi} + k_t T_{\xi ij} \hat{\xi}_\perp), \quad (3)$$

$$\mathbf{f}_{\eta ij} \equiv 2a(k_n N_{\eta ij} \hat{\eta} + k_t T_{\eta ij} \hat{\eta}_\perp), \quad (4)$$

where

$$N_{\xi ij} \equiv \partial_{i+}U_{ij}, \quad N_{\eta ij} \equiv \partial_{j+}V_{ij}, \quad (5)$$

$$T_{\xi ij} \equiv \frac{\partial_{i+}V_{ij} - \cos \alpha_0 \partial_{i+}U_{ij}}{\sin \alpha_0} - \frac{\Phi_{ij} + \Phi_{i+1j}}{2} - \Psi_{\xi ij}, \quad (6)$$

$$T_{\eta ij} \equiv \frac{\partial_{j+}U_{ij} - \cos \alpha_0 \partial_{j+}V_{ij}}{\sin \alpha_0} + \frac{\Phi_{ij} + \Phi_{ij+1}}{2} + \Psi_{\eta ij}. \quad (7)$$

The gravitational potential energy of particle (i, j) is $-mg \cdot \mathbf{U}_{ij} = m(g_\xi U_{ij} + g_\eta V_{ij})$, where $\mathbf{g} \equiv -g_\xi \hat{\xi} - g_\eta \hat{\eta}$ denotes the acceleration due to gravity.

A state of this system is represented by the set $\{\mathbf{S}_{ij}\}$, where $\mathbf{S}_{ij} \equiv (U_{ij}, V_{ij}, \Phi_{ij}, \Psi_{\xi ij}, \Psi_{\eta ij})$. We set $2a, m, k_n$ and g to 1 through the rescaling $\mathbf{x}_{ij} \rightarrow 2a\mathbf{x}_{ij}$, $k_t \rightarrow k_t k_n$, $\mathbf{g} \rightarrow g\mathbf{g}$ and $(U_{ij}, V_{ij}, 2a\Phi_{ij}, 2a\Psi_{\xi ij}, 2a\Psi_{\eta ij}) \rightarrow \frac{mg}{k_n} \mathbf{S}_{ij}$. As a result, the energy of the system is obtained as

$$E\{\mathbf{S}_{ij}\} = \sum_{ij} (E_{gij} + E_{eij}), \quad (8)$$

$$E_{gij} \equiv g_\xi U_{ij} + g_\eta V_{ij}, \quad (9)$$

$$E_{eij} \equiv \frac{1}{2}(N_{\xi ij}^2 + N_{\eta ij}^2) + \frac{1}{2}k_t(T_{\xi ij}^2 + T_{\eta ij}^2). \quad (10)$$

These equations are essentially the same as the equations of the DEM simulations for infinitesimal deformations under compressive stress [21]. We conjecture that the slip displacements $\Psi_{\xi ij}$ and $\Psi_{\eta ij}$ change quasi-statically with the boundary conditions. Therefore, the following equilibrium equations are obtained by differentiating E with respect to U_{ij}, V_{ij} and Φ_{ij} , with all values of the slip displacements fixed:

$$\partial_{i-}N_{\xi ij} + \frac{k_t}{\sin \alpha_0} (\partial_{j-}T_{\eta ij} - \cos \alpha_0 \partial_{i-}T_{\xi ij}) = g_\xi, \quad (11)$$

$$\partial_{j-}N_{\eta ij} + \frac{k_t}{\sin \alpha_0} (\partial_{i-}T_{\xi ij} - \cos \alpha_0 \partial_{j-}T_{\eta ij}) = g_\eta, \quad (12)$$

$$\left(1 - \frac{1}{2}\partial_{i-}\right)T_{\xi ij} = \left(1 - \frac{1}{2}\partial_{j-}\right)T_{\eta ij}. \quad (13)$$

Two particles in contact slip with respect to each other slightly at every time that the Coulomb conditions are broken as the boundary conditions change quasi-statically. For the two contacts of the particle (i, j) mentioned above, the Coulomb conditions are expressed as

$$k_t|T_{\xi ij}| \leq -\mu N_{\xi ij} \quad \text{and} \quad k_t|T_{\eta ij}| \leq -\mu N_{\eta ij}, \quad (14)$$

using the frictional coefficient μ . We ignore the details of the frictional interaction, such as the difference between the values of the static and dynamic frictional coefficients. Slip occurs in such a manner that the magnitude of the tangential elastic force is reduced at the contact. We obtain the update rules for the slip displacements $\Psi_{\xi ij}$ and $\Psi_{\eta ij}$ by enforcing the above Coulomb conditions at all contacts. When the Coulomb conditions are broken at some contact point, the slip displacement is updated to the value for which the equality is satisfied.

The state of the system, $\{\mathbf{S}_{ij}\}$, is determined from the equilibrium equations (11)-(13) and the update rules (14), under appropriate boundary conditions. All of the parameters that depend on the properties of the constituent particles are k_t and μ . We note that formally these equations do not change in the limit of hard particles, because the tangential spring constant k_t is rescaled by the normal spring constant k_n .

Note that the energy (8) is identical for all states related through the non-sliding mode, in which all particles rotate alternately in the clockwise and counterclockwise directions, according to $\Phi_{i+1j} = \Phi_{ij+1} = -\Phi_{ij}$. Although it is known that this mode is important when the boundaries of the system are time dependent [24-26], we believe that it is not important in quasi-static processes, because it is determined by the boundary conditions.

3 Numerical simulations

The results of our numerical simulations of the linearized model considered presently are consistent with those obtained previously from the DEM simulations [21]. Our numerical simulations of the linearized model were carried out by repeating the following three steps.

1. For given boundary conditions and slip displacements, we calculate the equilibrium state $(U_{ij}, V_{ij}, \Phi_{ij})$ by minimizing the energy (8) using the conjugate gradient method with a tolerance of 10^{-6} [29].

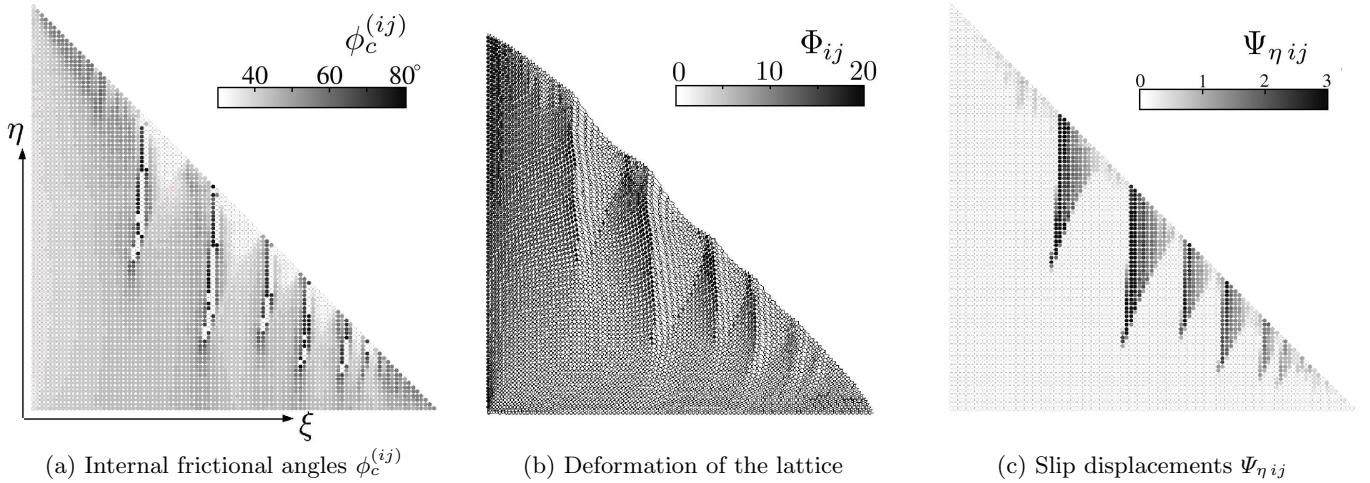


Fig. 3. Snapshots obtained from a numerical simulation with frictional coefficient $\mu = 0.5$.

2. We check the Coulomb conditions (14) for every particle and, if the conditions are broken, update the values of the slip displacements $\Psi_{\xi ij}$ and $\Psi_{\eta ij}$.
3. We increase the angle made by the V-walls. We denote this angle by α , where initially $\alpha = \alpha_0$, and express the rotation angle by $\theta \equiv 2ak_n(\alpha - \alpha_0)/mg$. With each increment, θ is increased by a value $\Delta\theta = 10^{-4}$ by rotating the right wall.

Here, we moved the boundary by rotating the right wall of the V-container in the clockwise direction, with the left wall fixed.

We prepared initial arrangements in which the tangential forces $k_t T_{\xi ij}$ and $k_t T_{\eta ij}$ vanish for every particle by choosing appropriate initial values for $\Psi_{\xi ij}$ and $\Psi_{\eta ij}$ at $\theta = 0$. The upper surface, where $i + j = L - 1$, is a free boundary. We assumed that, at each wall (i.e. $i = 0$ and $j = 0$), particles are fixed in the normal direction and move freely along the wall. The results of the numerical simulations were found to be insensitive to details of the boundary conditions at the walls. In particular, they do not change qualitatively when we used fixed boundary conditions.

Figure 3 displays the three kinds of snapshots obtained at $\theta = 20$ from a numerical simulation using the parameter values $L = 100$, $k_t = 0.1$, $\mu = 0.5$ and $\phi_g = -15^\circ$. In these snapshots, ξ and η are displayed as orthogonal, although in fact we used $\alpha_0 = 60^\circ$ here. We note that the parameters k_n , a , m and g are not contained in this model, and the arrangement of particles is rhombic even in the case of $\alpha_0 = 60^\circ$. The results do not change qualitatively if either α_0 or ϕ_g is varied by several degrees. Figure 3(a) is a gray-scale image of the internal frictional angles $\phi_c^{(ij)}$ in the system, where $\phi_c^{(ij)}$ is calculated from the equation $\cos \phi_c^{(ij)} = 2\sqrt{\det \sigma^{(ij)}} / |\text{Tr} \sigma^{(ij)}|$ by defining the stress tensor of the particle (i, j) as $\sigma^{(ij)} \equiv \frac{1}{2}\{(\mathbf{f}_{\xi ij} + \mathbf{f}_{\xi i+1j})\hat{\xi} + (\mathbf{f}_{\eta ij} + \mathbf{f}_{\eta i+1j})\hat{\eta}\}$ [13]. Figure 3(b) depicts the deformation of the lattice, which is drawn with an appropriate scale, after subtracting the initial deformation and a uniform shear deformation. The shading of the small circle positioned at each site represents the rotation angle Φ_{ij} . Here, for a counterclockwise rotation, the

shading becomes darker as the magnitude of the rotation increases, while for any clockwise rotation, the circle is white. Figure 3(c) displays a gray-scale image of the slip displacements $\Psi_{\eta ij}$. We note that $\Psi_{\eta ij}$ here represents the total slippage distance from the initial state, not that for the present time step alone. In many areas of nonvanishing $\Psi_{\eta ij}$, in fact there was no slip in the present time step.

As the wall is rotated, microscopic shear zones appear from the vicinity of the surface, and, as a result of competitive growth, some of them survive and grow in length. The microscopic shear zones are approximately parallel to the η direction when ϕ_g is negative, that is, when $g_\eta < g_\xi$. In these shear zones, the slip displacements $\Psi_{\eta ij}$ increase with the rotation of the wall, while the values $\Psi_{\xi ij}$ do not change. Particles slip at the contact points positioned along the η direction. Contrastingly, they roll without sliding at the contacts positioned along the ξ direction. These results are consistent with those obtained from our previous work.

We observed that the elastic compressive forces along the η direction, $|N_{\eta ij}|$, decrease along these shear zones as the wall rotates. Such decreasing makes it easier for the second Coulomb condition of Eq. (14) to be broken. For this reason, the direction of the microscopic shear zones is inclined toward the minimum principal axis of stress rather than the maximum principal axis. As the wall rotates further, $N_{\eta ij}$ becomes positive at some contact points in the developed shear zones. Because it is impossible for the interactions between particles in dry granular systems to become attractive, we infer that these contacts are lost, as observed in the DEM simulations. We, however, believe that this is unimportant in the initial deformation process, because the number of such points is small.

The microscopic shear zones migrate in the ξ direction, while growing in length in the η direction. The triangular gray regions of nonvanishing $\Psi_{\eta ij}$ in Fig. 3(c) appear as a result of such migrations. The migration distance decreases with the frictional coefficient μ . Figure 4 displays a gray-scale image of the slip displacements $\Psi_{\eta ij}$ obtained using a smaller coefficient, $\mu = 0.1$.

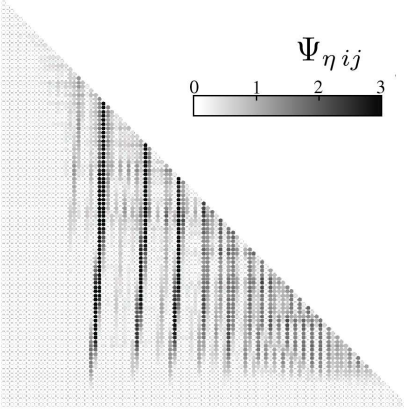


Fig. 4. A snapshot of slip displacements obtained from a numerical simulation using $\mu = 0.1$.

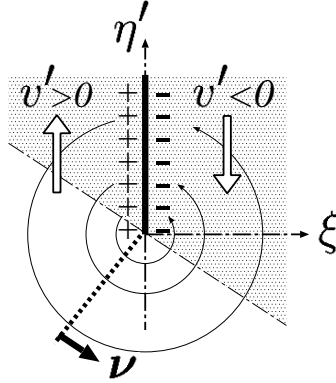


Fig. 5. The deformation field caused by a single shear zone.

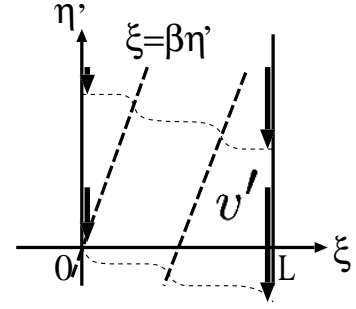


Fig. 6. The 1-d perturbation of the critical state used in the stability analysis. The contours of the displacement v' correspond to $\xi = \beta'\eta + \text{const.}$

4

Perturbative analysis

In order to investigate Eqs. (11)-(14) analytically, we first derive the leading-order terms of these equations in the limit of small tangential interactions. We express the change of state from the initial state $\mathbf{S}_{ij} = (U_{ij}^0, V_{ij}^0, 0, \Psi_{\xi ij}^0, \Psi_{\eta ij}^0)$ as $\mathbf{s}_{ij} \equiv (u_{ij}, v_{ij}, \phi_{ij}, 0, \psi_{\eta ij})$. Assuming that $\Psi_{\xi ij}$ does not change at any contact, we consider the simple case in which microscopic shear zones develop approximately parallel to the η axis, as mentioned in the previous section. We assume that this disturbance changes slowly along the η direction in comparison to the ξ direction in this limit.

The initial state is determined by the equilibrium equations, $\partial_i N_{\xi ij}^0 = g_{\xi}$, $\partial_j N_{\eta ij}^0 = g_{\eta}$ and $T_{\xi ij}^0 = T_{\eta ij}^0 = 0$, where $N_{\xi ij}^0$, $N_{\eta ij}^0$, $T_{\xi ij}^0$ and $T_{\eta ij}^0$ represent the initial contact forces defined by Eqs. (5)-(7). The quantities $N_{\xi ij}^0$ and $N_{\eta ij}^0$ are negative and decrease with the distance from the free surface as $N_{\eta ij}^0 = -g_{\eta}(L - 1 - i - j)$.

The equilibrium equations with respect to $u_{ij}, v_{ij}, \phi_{ij}$ and $\psi_{\eta ij}$ are linear and homogeneous. They are obtained from Eqs. (11)-(13), and their left-hand sides are the same as those of the original equations, except that \mathbf{S}_{ij} is replaced by \mathbf{s}_{ij} . Introducing a small parameter ϵ in term of which to carry out the perturbative analysis, we assume that the differences $\partial_{i\pm}$ and $\partial_{j\pm}$ of these variables are order 1 and ϵ , respectively. We first determine the orders of the variables contained in the equations as follows. The results of the numerical simulations indicate that the change of the elastic force $N_{\eta ij}$, i.e. $\partial_{j+} v_{ij}$, becomes of the same order as the initial value $N_{\eta ij}^0$ along microscopic shear zones. Because $N_{\eta ij}^0$ is independent of ϵ , we assume that the displacements v_{ij} are order ϵ^{-1} . Local shear strains in microscopic shear zones induce slips and rotations of particles. Therefore, ϕ_{ij} and $\psi_{\eta ij}$ are expected to be of the same order as $\partial_{i+} v_{ij}$, that is, ϵ^{-1} . Using these estimations, we investigate the equilibrium equations derived from Eqs. (11) and (12). In order to balance the two terms in each equation, the parameter k_t and the displacement u_{ij} must satisfy $k_t \sim \epsilon^2$ and $u_{ij} \sim k_t v_{ij} \sim \epsilon$. Similar consideration leads us to conclude that μ should be order ϵ

to balance both sides of the second Coulomb condition in Eq. (14). These order estimates of k_t and μ indicate that the tangential interactions among particles decrease with ϵ .

Assuming that $k_t \sim \epsilon^2$, $\mu \sim \epsilon$, $v_{ij}, \psi_{\eta ij}, \phi_{ij} \sim \epsilon^{-1}$ and $u_{ij} \sim \epsilon$, based on the above arguments, we extract the terms of lowest order in ϵ from the equilibrium equations. From Eqs. (6) and (7), we obtain

$$T_{\xi ij} = \frac{\partial_{i+} v_{ij}}{\sin \alpha_0} - \left(1 + \frac{1}{2} \partial_{i+}\right) \phi_{ij}, \quad (15)$$

$$T_{\eta ij} = \phi_{ij} + \psi_{\eta ij}. \quad (16)$$

The equilibrium equations (11)-(13) are reduced to

$$\partial_i \partial_{i+} u_{ij} - \frac{k_t}{\tan \alpha_0} \partial_i T_{\xi ij} = 0, \quad (17)$$

$$\partial_j \partial_{j+} v_{ij} + \frac{k_t}{\sin \alpha_0} \partial_i T_{\xi ij} = 0, \quad (18)$$

$$\left(1 - \frac{1}{2} \partial_{i-}\right) T_{\xi ij} = T_{\eta ij}, \quad (19)$$

and, from the second condition in Eq. (14), the Coulomb condition is expressed as

$$\mu (N_{\eta ij}^0 + \partial_{j+} v_{ij}) \leq k_t T_{\eta ij}. \quad (20)$$

Here, we have chosen the sign of $T_{\eta ij}$ to be negative so that it corresponds to the situation in our numerical simulations.

Excluding Eq. (17), Eqs. (18)-(20) are closed with respect to the three variables v_{ij}, ϕ_{ij} and $\psi_{\eta ij}$. We treat these variables as continuous functions, $v_i(\eta)$, $\phi_i(\eta)$ and $\psi_{\eta i}(\eta)$, and approximate the finite difference in the η direction, $\partial_{j\pm}$, by the differentiation operator ∂_{η} . It is convenient to introduce the new variables

$$v'_i \equiv \frac{v_i}{\sin \alpha_0} \quad \text{and} \quad \eta' \equiv \sqrt{\frac{k_t}{2}} \frac{\eta}{\sin \alpha_0}. \quad (21)$$

Then, substituting Eqs. (15) and (16) into Eq. (19), we obtain the equation

$$2I_i \phi_i = \partial_i v'_i - \psi_{\eta i}, \quad (22)$$

where we have defined the finite differential operators

$$I_i \equiv 1 + \frac{1}{8} \partial_{i-} \partial_{i+} \quad \text{and} \quad \partial_i v'_i \equiv \frac{1}{2} (v'_{i+1} - v'_{i-1}). \quad (23)$$

Because the Fourier transform of I_i is finite for any mode, we can solve the above equation formally by introducing

the inverse operator I_i^{-1} . Substituting it into Eqs. (18) and (20), we finally obtain the following equations:

$$(\partial_{\eta'}^2 I_i + \partial_{i-} \partial_{i+}) v'_i = -\partial_i \psi_{\eta i}, \quad (24)$$

$$N'_{\eta i}{}^0 + (\mu' \partial_{\eta'} - I_i^{-1} \partial_i) v'_i \leq (2 - I_i^{-1}) \psi_{\eta i}, \quad (25)$$

where

$$\mu' \equiv \sqrt{\frac{2}{k_t}} \mu \quad \text{and} \quad N'_{\eta i}{}^0 \equiv \frac{2\mu}{k_t} N_{\eta i}{}^0. \quad (26)$$

These equations are closed with respect to v'_i and $\psi_{\eta i}$. The slip displacement $\psi_{\eta i}$ deforms the lattice around the contact point in the direction of $\hat{\xi}_\perp$, and the deformation v'_i affects the slip condition at each contact. The function $N'_{\eta i}{}^0(\eta)$ is determined by the initial conditions. We find that the behavior of the system in the case of small deformations is essentially determined by the parameter μ' for given initial and boundary conditions.

As a first application of the simplified equations derived above, we investigate the effect of uniform shear deformation caused by the rotating wall. To lowest order in ϵ , the boundary conditions used in our numerical simulations are written $\partial_{\eta'} v'_i = 0$ on the free surface and $v'_i(0) = -\theta i$ on the ξ axis. When no slip appears of any contact (i.e., $\psi_{\eta i} = 0$), uniform shear deformation represented by $v'_i(\eta) = -\theta i$ is the solution of Eq. (24) satisfying these boundary conditions. Substituting this solution into the Coulomb condition (25), we obtain $N'_{\eta i}{}^0 + \theta \leq 0$. As the angle of the wall θ increases, particles begin to slip at the contacts where this condition is broken. Because $N'_{\eta i}{}^0$ decreases as the distance from the free surface increases, we find that the slip region appears from the vicinity of the free surface.

We next consider the long wavelength limit of Eqs. (24) and (25) with respect to ξ by replacing the operator I_i by 1. Then, we treat the variables as continuous functions $v'(\xi, \eta')$, $\psi_\eta(\xi, \eta')$ and $N'_\eta{}^0(\xi, \eta')$ and approximate $\partial_{i\pm}$ by the differentiation operator ∂_ξ . The left-hand side of Eq. (24) becomes $(\partial_{\eta'}^2 + \partial_\xi^2) v' \equiv \Delta v'$. Therefore, the displacement v' is analogous to an electrostatic potential when we regard the slip displacement ψ_η as the density of dipoles pointing in the negative ξ direction. Defining the ‘‘electric field’’ $\mathbf{E}' \equiv -(\partial_\xi v', \partial_{\eta'} v')$ and the vector $\boldsymbol{\nu} \equiv (1, -\mu')$, the approximate forms of Eqs. (24) and (25) in this limit are

$$\Delta v' = -\partial_\xi \psi_\eta \quad \text{and} \quad N'_\eta{}^0 + \boldsymbol{\nu} \cdot \mathbf{E}' \leq \psi_\eta. \quad (27)$$

We believe that with regard to the qualitative behavior of solutions, these are the same as the original equations, although they are not correct quantitatively in the vicinity of microscopic shear zones.

The above equations are similar to those describing the dielectric breakdown problem. It is known that a fingering-like pattern appears in the spatial distribution of the dielectric constant $\epsilon_e(\mathbf{r})$ in the system considered in that problem. For a given $\epsilon_e(\mathbf{r})$, the electric potential $v_e(\mathbf{r})$ is determined by the equation $\nabla \cdot (\epsilon_e \nabla v_e) = 0$ [30]. Electric breakdown caused by a strong electric field increases the value of $\epsilon_e(\mathbf{r})$. We here assume that a uniform electric field E_0 exists initially in the negative x direction. Then, if the

change of the potential, $v'_e(\mathbf{r}) \equiv v_e(\mathbf{r}) - E_0 x$, is sufficiently small, this equation can be approximated as

$$\Delta v'_e = -\nabla v_e \cdot \nabla \log \epsilon_e \simeq -\partial_x \psi_e, \quad \text{where } \psi_e \equiv E_0 \log \epsilon_e. \quad (28)$$

This has the same form as the first equation of Eq. (27). Therefore, we can regard the development of heterogeneity in the stress field as a kind of breakdown phenomenon.

We now investigate the deformation caused by a straight shear zone using Eq.(27). We assume the semi-infinite slip displacement $\psi' = K\delta(\xi)\Theta(\eta')$ in an infinite system (as depicted in Fig. 5), where K is a positive constant and $\Theta(x)$ is the Heaviside function. The solution is

$$\mathbf{E}' = (K/2\pi r'^2)(-\eta', \xi). \quad (29)$$

Here, we have defined the distance from the tip of the shear zone as $r' \equiv \sqrt{\xi^2 + \eta'^2}$. The stress field decays in a form inversely proportional to r' . We note that this dependence differs from that of a crack in elastic materials, although shear zones in granular systems natively appear to be similar to mode-II cracks in the long-range effect to the stress field. When a shear zone develops, new slip is inhibited in the region satisfying $\boldsymbol{\nu} \cdot \mathbf{E}' < 0$, behind the tip. We infer that such a screening effect causes competitive growth of microscopic shear zones. In contrast, we conjecture that the shear zone develops in the direction of the largest value of $\boldsymbol{\nu} \cdot \mathbf{E}'$ from the tip. This direction tilts from the η axis as μ' increases. This suggests that the migration distance of microscopic shear zones in the ξ direction increases as a function of the frictional coefficient μ .

We finally show that the critical stress state of this system is unstable with respect to simple shear deformation. In the critical stress state, the particles in the system slip uniformly, so that the equality in the Coulomb condition holds at every contact. In this case, substituting the second equation of Eq. (27) into the first, we obtain the hyperbolic equation

$$\partial_{\eta'}(\partial_{\eta'} + \mu' \partial_\xi) v' = -\partial_\xi N'_\eta{}^0. \quad (30)$$

The critical state is determined by this equation. Here, we apply the simple shear boundary condition $v'(L, \eta') - v'(0, \eta') = -\theta L$ to an infinite system along the η direction, as depicted in Fig. 6. Assuming that a series of microscopic shear zones tilted by a slope β from the η axis develops as a result of instability, we investigate the case in which the perturbations from the critical stress state, $\delta v'$ and $\delta \psi_\eta$, can be expressed as functions of the single variable $\xi - \beta \eta'$. Then, from Eq. (27), we obtain the equations for $\delta v'$ and $\delta \psi_\eta$:

$$(\beta^2 + 1)\partial_\xi^2 \delta v' = -\partial_\xi \delta \psi_\eta \quad \text{and} \quad -(\mu' \beta + 1)\partial_\xi \delta v' \leq \delta \psi_\eta. \quad (31)$$

The slip displacement $\delta \psi_\eta$ increases if the second condition here is broken. We integrate the first equation, employing the boundary condition $\delta v'(L, \eta') - \delta v'(0, \eta') = 0$, and obtain the solution

$$(\beta^2 + 1)\partial_\xi \delta v' = \langle \delta \psi_\eta \rangle - \delta \psi_\eta, \quad (32)$$

where $\langle \delta \psi_\eta \rangle \equiv \frac{1}{L} \int_0^L d\xi \delta \psi_\eta$. Substituting this solution into the second condition in Eq. (31), the Coulomb condition is obtained in terms of $\delta \psi_\eta$ alone as

$$\beta(\mu' - \beta)\delta \psi_\eta \leq (1 + \mu' \beta)\langle \delta \psi_\eta \rangle. \quad (33)$$

No slip occurs if $\delta \psi_\eta$ satisfies this inequality everywhere. In particular, for $0 < \beta < \mu'$, this condition gives the upper threshold of $\delta \psi_\eta$ for stability, and if $\delta \psi_\eta$ is larger than the threshold somewhere, the perturbation is inferred to

grow. For a slope $\beta = (-1 + \sqrt{1 + \mu'^2})/\mu' \equiv \beta_c$, this upper threshold is smallest for a given spatial average $\langle \delta\psi_\eta \rangle$, and Eq. (33) can be rewritten

$$\delta\psi_\eta \leq \frac{1}{\beta_c^2} \langle \delta\psi_\eta \rangle. \quad (34)$$

Thus the critical stress state is unstable with respect to a finite perturbation. We note that β_c is an increasing function of μ' and approaches 1. The threshold decreases as the frictional coefficient μ increases. In the case that a non-vanishing area of $\delta\psi_\eta$ is localized in the system, the spatial average $\langle \delta\psi_\eta \rangle$ decreases as the area becomes smaller. Therefore, a single localized zone appearing in the critical state always develops in a large system.

5

Conclusions

We investigated quasi-static deformation processes in idealized systems with regular arrangements of identical particles. The purpose of this study was to understand the role of frictional interactions between constituent particles in the dynamics. For infinitesimal deformations of such systems, we proposed a lattice model linearized with respect to the displacements of particles. We introduced slip displacements of particles in contact as new variables in this model and considered Coulomb friction. It should be noted that some information about the history of the deformation is preserved in the form of the slip displacements. The numerical simulations show that the stress field and the slip displacements develop heterogeneously when a shear deformation is applied to the system, as found in the previous DEM simulations. We found that microscopic shear zones appear through a fingering-like instability of the stress field, and some of them grow in length while migrating in the direction perpendicular to the direction of their growth.

In the limit of small tangential interactions, we derived approximate equations from this model using a perturbative analysis. In the long wavelength limit, these equations are analogous to a model of dielectric breakdown. Through this analogy we can interpret the slip displacement as a dipole density and the displacement of each particle as an electric potential. On the basis of these equations, we studied the screening effect of a single microscopic shear zone and the stability of the critical stress state.

We expect that these results shed light on the dynamics of microbands [15] and the creation process of shear bands. The creation process in actual granular systems is more complicated because the arrangements of particles are irregular. It is a subject for a further study to investigate the effect of the size distribution of particles to the dynamics of quasi-static deformation.

It is a pleasure to acknowledge H. Hayakawa and C. Urabe for fruitful discussions. We thank G. C. Paquette for reading the manuscript conscientiously. This study is supported by a Grant-in-Aid from the Japan Science and Technology Corporation.

Notation

$\xi \equiv 2ai$ and $\eta \equiv 2aj$ are the reference coordinates along the walls in the initial state. The subscript ij and the superscript (ij) denote values of the particle (i, j) , and the subscript i denotes values of continuous functions with respect to η at $\xi = 2ai$. The superscript 0 denotes initial values.

The finite differential operators $\partial_{i\pm} A_{ij} \equiv \pm(A_{i\pm 1j} - A_{ij})/2a$ and $\partial_{j\pm} A_{ij} \equiv \pm(A_{ij\pm 1} - A_{ij})/2a$ are defined. I_i and ∂_i are defined by Eq.(23).

The list of symbols below gives those which appear in two or more paragraphs.

$\hat{\xi}, \hat{\eta}$	Unit vectors in the ξ and η directions
$\hat{\xi}_\perp, \hat{\eta}_\perp$	Inward unit vectors perpendicular to $\hat{\xi}$ and $\hat{\eta}$
a	Radius of a particle
m	Mass of a particle
x	Reference position of a particle
g	Acceleration due to gravity
g_ξ, g_η	$g \equiv -g_\xi \hat{\xi} - g_\eta \hat{\eta}$
ϕ_g	Angle of the x axis bisecting the V-shaped container with respect to g
μ	frictional coefficient
k_n, k_t	Normal and tangential spring constants
α	Angle made by the V-walls
θ	$\theta \equiv 2ak_n(\alpha - \alpha_0)/mg$
L	System size (number of particles along a wall)
U	Displacement of a particle
U, V	ξ and η components of U
Φ	Rotation angle of a particle
Ψ_ξ, Ψ_η	Slip displacements divided by $2a$
S	State of a particle, $S \equiv (U, V, \Phi, \Psi_\xi, \Psi_\eta)$
f_ξ, f_η	Elastic forces acting on a particle
N_ξ, N_η	Normal components of f_ξ and f_η
T_ξ, T_η	Tangential components of f_ξ and f_η
u, v, ϕ, ψ_η	Change of U, V, Φ, Ψ_η from the initial state
s	Change of state, $s \equiv (u, v, \phi, 0, \psi_\eta)$
ϵ	Small parameter for the perturbative analysis
v', η'	Variables defined by Eq.(21)
μ', N'_η	Parameter and variable defined by Eq.(26)
E'	$E' \equiv -(\partial_\xi v', \partial_\eta v')$
ν	$\nu \equiv (1, -\mu')$

References

1. D. M. Wood, *Soil Behaviour and Critical State Soil Mechanics* (Cambridge University Press, New York, 1990)
2. R. M. Nedderman, *Statics and Kinematics of Granular Materials* (Cambridge University Press, Cambridge, 1992)
3. A. N. B. Poliakov & H. J. Herrmann, *Geophys. Res. Lett.* **21** (1994), p. 2143
4. H. M. Jaeger, S. R. Nagel & R. P. Behringer, *Rev. Mod. Phys.* **68** (1996), p. 1259
5. P. G. de Gennes, *Physica A* **261** (1998), p. 267
6. P. Claudin, J. -P. Bouchaud, M. E. Cates & J. P. Wittmer, *Phys. Rev. E* **57** (1998), p. 4441
7. L. Vanel, D. Howell, D. Clark, R. P. Behringer & E. Clément, *Phys. Rev. E* **60** (1999), p. R5040

8. J. Geng, D. Howell, E. Longhi, R. P. Behringer, G. Reydellet, L. Vanel, E. Clément & S. Luding, *Phys. Rev. Lett.* **87** (2001), p. 35506
9. J. -P. Bouchaud, P. Claudin, D. Levine & M. Otto, *Eur. Phys. J. E* **4** (2001), p. 451
10. C. Thornton & S. J. Antony, *Phil. Trans. R. Soc. Lond. A* **356** (1998), p. 2763
11. C. Thornton & S. J. Antony, *Powder Technology* **109** (2000), p. 179
12. J. A. Åström, H. J. Herrmann & J. Timonen, *Phys. Rev. Lett.* **84** (2000), p. 638
13. M. Lätzel, S. Luding & H. Herrmann, *Granular Matter* **2** (2000), p. 123
14. J. R. Williams & N. Rege, *Powder Technol.* **90** (1997), p. 187
15. M. R. Kuhn, *Mech. Mater.* **31** (1999), p. 407
16. M. R. Kuhn, *Granular Matter* **4** (2003), p. 155
17. J. -N. Roux & G. Combe, *C. R. Phys.* **3** (2002), p. 131
18. T. Terada & N. Miyabe, *Bull. Earthq. Res. Inst.* **4** (1928), p. 33; **6** (1929), p. 109; **7** (1929), p. 65
19. M. K. Hubbert, *Bull. Geol. Soc. Am.* **62** (1951), p. 355
20. H. Wolf, D. König & T. Triantafyllidis, *J. Struct. Geol.* **25** (2003), p. 1229
21. S. Kitsunozaki & A. Kurumatani, *Granular Matter* **5** (2004), p. 185
22. P. A. Cundall & O. D. L. Strack, *Géotechnique* **29** (1979), p. 47
23. C. Goldenberg and I. Goldhirsch, *Phys. Rev. Lett.* **89** (2002), p. 084302-1
24. F. Radjai & S. Roux, *Phys. Rev. E* **51** (1995), p. 6177
25. F. Radjai, P. Evesque, D. Bideau & S. Roux, *Phys. Rev. E* **52** (1995), p. 5555
26. F. Radjai, L. Brendel & S. Roux, *Phys. Rev. E* **54** (1996), p. 861
27. G. Schliecker, Y. Khidas, M. Ammi & J. -C. Messenger, *Phys. Rev. E* **62** (2000), p. 744
28. J. Duran, *Sands, Powders and Grains* (Springer-Verlag, New York, 2000)
29. W. H. Press, B. P. Flannery, S. A. Teukolsky & W. T. Vetterling, *Numerical Recipes* (Cambridge University Press, New York, 1997)
30. B. K. Chakrabarti & L. G. Benguigui, *Statistical Physics of Fracture and Breakdown in Disordered Systems* (Oxford University Press, New York, 1997)